



HAL
open science

On the use of Zonal Immersed Boundaries on the FG5 missile configuration

Lucas Manueco, Pierre-Élie Weiss, Sébastien Deck

► **To cite this version:**

Lucas Manueco, Pierre-Élie Weiss, Sébastien Deck. On the use of Zonal Immersed Boundaries on the FG5 missile configuration. 55th 3AF International conference on Applied Aerodynamics, Mar 2020, Poitiers, France. hal-03228534

HAL Id: hal-03228534

<https://hal.science/hal-03228534>

Submitted on 18 May 2021

HAL is a multi-disciplinary open access archive for the deposit and dissemination of scientific research documents, whether they are published or not. The documents may come from teaching and research institutions in France or abroad, or from public or private research centers.

L'archive ouverte pluridisciplinaire **HAL**, est destinée au dépôt et à la diffusion de documents scientifiques de niveau recherche, publiés ou non, émanant des établissements d'enseignement et de recherche français ou étrangers, des laboratoires publics ou privés.

On the use of Zonal Immersed Boundaries on the FG5 missile configuration

Lucas Manueco⁽¹⁾, Pierre-Élie Weiss⁽²⁾ and Sébastien Deck⁽³⁾

⁽¹⁾Ph.D. Student, ONERA, Paris-Saclay University, F-92190 Meudon - France, lucas.manueco@onera.fr

⁽²⁾Research Scientist, ONERA, Paris-Saclay University, F-92190 Meudon - France, pierre-elie.weiss@onera.fr

⁽³⁾Research Scientist, ONERA, Paris-Saclay University, F-92190 Meudon - France, sebastien.deck@onera.fr

ABSTRACT

One of the major problems in applied aerodynamics remains the representativeness of the flow around complex geometries, especially for unsteady numerical simulations. In this context, Weiss and Deck [26] proposed to use both Immersed Boundary Conditions (IBC) and body-fitted (BF) boundary conditions to simulate a full-space launcher. This approach, named Zonal Immersed Boundary Conditions (ZIBC), takes advantage of IBC to add complex geometrical details in simple body-fitted configurations. So far, this approach has been used with the IBC formulation presented by Mochel *et al.* [16]. The present paper introduces a new IBC formulation inside the ZIBC framework based on a sharp surface reconstruction approach. Moreover, a wall model is coupled with the IBC to reduce the mesh requirements related to accurate prediction of turbulent boundary layers. The purpose of these additions is to extend the use of IBC for the simulation of technological details in attached flow regions. A FG5 missile configuration is computed using ZIBC at a Mach number of 0.8 and an angle of attack of 10°. For this configuration, the fuselage is modelled using a body-fitted grid, and the wings are introduced with the new IBC formulation. The accuracy of the current approach is assessed comparing a full body-fitted simulation with the available experimental data.

1. INTRODUCTION

The generation of a suitable mesh in CFD is still one of the most challenging and time-consuming tasks for the simulation of industrial geometries. In addition to the complexity of the process, the introduction of sharp and complex geometrical details can result in a grid made up with highly anisotropic and skewed cells which reduce the mesh quality for both structured and unstruc-

tured meshing techniques locally. As a consequence, the accuracy and the robustness of the CFD simulations can be dramatically decreased. This issue is even more constraining when it comes to unsteady simulations since the global time step is generally limited by the most skewed cells to ensure a stable computation.

In this framework, Immersed Boundary Conditions (IBC) have shown to be a useful tool to simulate complex geometries for compressible turbulent flows. The wall boundary condition is enforced through the application of source terms allowing to uncouple the mesh and the geometry. Mochel *et al.* [16] demonstrate the capacity of the zonal use of immersed boundaries, to introduce a control device on an afterbody flow. Afterwards, the same methodology, namely the Zonal Immersed Boundary Conditions (IBC), has been used by Weiss and Deck [26] for the simulation of the Ariane 5 space launcher. In this latter study the IBC approach is mainly used to generate a blockage effect in the flow and not to predict attached flows.

The correct simulation of the near-wall attached flow would require isotropic mesh refinement around immersed boundaries, which is generally too expensive for 3D compressible flows. As a consequence, wall models are often coupled with IBC to improve their capability to simulate attached boundary layers. In the past years, numerous wall models have been proposed to improve IBC formulation [3, 4]. Among these approaches, Thin Boundary Layer Equations (TBLE) based wall models have shown to correctly predict highly compressible flows and can be coupled with turbulence models.

The object of this paper is to modify the immersed boundary formulation used in the ZIBC approach to properly reproduce the effect of complex details on a flow in which boundary layers may potentially develop. This IBC is based on a direct forcing approach with a reconstruction procedure which uses both cell and face forcing.

Moreover, it is combined with a TBLE-based wall model including a one-dimensional compressible version of the Spalart-Allmaras RANS model. These numerical methods are assessed for the simulation of the external transonic flow around the FG5 missile configuration with an angle of attack of 10° . The results are compared with full body-fitted simulation and with ONERA's experiments to investigate the accuracy of the new IBC approach. The paper is organized as follows. Section 2 presents the numerical aspects of the flow solver. Section 3 and 4 introduce the compact immersed boundary approach and the wall model presently used, respectively. Then, section 5 describes the FG5 test case. Finally, section 6 presents the RANS simulation around the configuration and a discussion of the results.

2. FLOW SOLVER

The simulations are performed with the FLU3M cell-center finite volume code. The code solves the Navier-Stokes equations on multi-block structured grids. This solver has been assessed for various applications and is primarily used for the simulation of transonic flow around space launchers such as the Ariane 6 PPH [25]. The RANS simulations are made with a compressible form of the Spalart-Allmaras model [26]. A Roe scheme with the Harten correction is used to compute the convective fluxes with a MUSCL reconstruction procedure to increase their spatial accuracy. The gradients in the Spalart-Allmaras RANS model and the diffusive fluxes are evaluated using the Green-Gauss method.

The computation of the diffusive fluxes with the Green-Gauss method can introduce numerical oscillations when the diffusive terms become dominant over convective terms. In one dimension, the sum of the diffusive fluxes \mathbf{F}_d applied to a given cell i can be written:

$$\sum_{l=1}^2 (\mathbf{F}_d)_{l,i} = \mathbf{W}_{i-2} \cdot K_{i-2} - 2 \cdot \mathbf{W}_i \cdot K_i + \mathbf{W}_{i+2} \cdot K_{i+2} \quad (1)$$

Where K_i stands for the volume and surface terms used to compute the diffusive fluxes with a Green-Gauss approach in cell i , which are here assumed constant for each cell as it would be in cartesian grids. \mathbf{W} represents the conservative variable vector. $\sum_{l=2}^6 (\mathbf{F}_d)_{l,i}$ does not depend on its direct neighbourhood. As a consequence, a strong even-odd decoupling oscillation can occur when the convective fluxes \mathbf{F}_c are negligible. This situation can occur inside turbulent boundary layers or in mixing layers. In a finite volume context, Chakravarthy [8] proposed to compute the diffusive fluxes with a Green-Gauss approach centred on each face as presented in fig. 2. Since the cell-center gradients are still required for the source terms of the RANS equation, an intermediate approach is used. First, the cell-center gradients are com-

puted with the Green-Gauss approach and stored. These gradients are required by the constitutive RANS model. Then a correction term is applied during the computation of the diffusive flux for each interface to retrieve the face center gradient of Chakravarthy [8]. This approach only needs to store the cell-center gradients and removes the even-odd decoupling phenomena caused by the diffusive fluxes. The new diffusive fluxes after this correction can be rewritten as:

$$\sum_{l=1}^2 (\mathbf{F}_d)_{l,i} = \mathbf{W}_{i-1} \cdot K'_{i-1} - 2 \cdot \mathbf{W}_i \cdot K'_i + \mathbf{W}_{i+1} \cdot K'_{i+1} \quad (2)$$

Where K' includes the new volume and surface terms used to compute the diffusive fluxes with the face center gradient of Chakravarthy [8].

Finally, the time discretization is achieved with the implicit and second-order accurate Gear scheme. This scheme is associated to a Newton-type iterative algorithm. The discrete finite volume system is defined as follows:

$$\frac{3}{2} \mathbf{W}^{n+1} - 2 \mathbf{W}^n - \frac{1}{2} \mathbf{W}^{n-1} = -\frac{\Delta t}{\Omega} \left(\sum_{l=1}^6 [(\mathbf{F}_c)_l - (\mathbf{F}_d)_l]^{n+1} - [\mathbf{T}_{\text{RANS}}]^{n+1} - [\mathbf{T}_{\text{IBC}}]^{n+1} \right) \quad (3)$$

where \mathbf{W}^n is the conservative variable vector at the iteration n , Ω the volume of a cell and \mathbf{T} the source terms for the IB forcing and the turbulence model. In the present work, $[\mathbf{T}_{\text{IBC}}]^{n+1}$ is decomposed into two parts with $[\mathbf{T}_{\text{IBC}}^{\text{solid}}]^{n+1}$ and $[\mathbf{T}_{\text{IBC}}^{\text{forcing}}]^{n+1}$ which are defined as follows:

$$[\mathbf{T}_{\text{IBC}}^{\text{solid}}]^{n+1} = {}^t \left(0, \text{tagibc} \times f_{\rho u_i}^{n+1}, 0, \text{tagibc} \times f_{\rho v}^{n+1} \right) \quad (4)$$

$$[\mathbf{T}_{\text{IBC}}^{\text{forcing}}]^{n+1} = {}^t \left(\alpha \times \left(\frac{\mathbf{W}^n - \mathbf{W}_F}{\Delta t} \Omega + \mathbf{f}_W^{n+1} \right) \right) \quad (5)$$

With \mathbf{f}_W^{n+1} the sum of the convective and diffusive fluxes, $\sum_{l=1}^6 [(\mathbf{F}_c)_l - (\mathbf{F}_d)_l]^{n+1}$ and \mathbf{W}_F the conservative variable vector given by the IBC formulation to enforce the boundary condition. The sensor *tagibc* is equal to 1 inside the immersed solid and 0 outside. $\mathbf{T}_{\text{IBC}}^{\text{solid}}$ corresponds to the initial IBC source terms proposed by Mochel et al. [16]. This source term is computationally inexpensive and is kept in the current implementation of the compact IBC to avoid the development of any flow in the immersed solid. Further details concerning the implementation of $\mathbf{T}_{\text{IBC}}^{\text{solid}}$, the discretization of the Immersed Boundary and the FLU3M solver can be found in Weiss and Deck [26]. The compact IBC approach presented in this article uses near-wall fluid cells to represent the immersed geometry sharply. Similarly, at *tagibc*, the sensor α is equal to 1 on the forcing cells presented in fig. 1 and 0 for the fluid and solid cells.

3. COMPACT IMMERSED BOUNDARY CONDITIONS

The present compact IBC is based on the direct forcing approach introduced by Mohd-Yusof [17]. As proposed by Fadlun et al. [11] a discrete reconstruction procedure is carried out on the fluid variable in order to compute \mathbf{W}_F and $\mathbf{T}_{IBC}^{\text{forcing}}$. This procedure is applied to near-wall forcing cells as represented in figure 1 and results in a sharper representation of the immersed boundary. To proceed to the reconstruction it is required to retrieve information from the surrounding flow field. Therefore, for each forcing cell, the conservative variables are reconstructed at an Interpolation Point (*IntP*) chosen in the wall normal direction (see fig. 1). A boundary formulation, represented by f_{IBC} , is used to describe the evolution of the conservative variable between the forcing and the interpolation points. This function f_{IBC} can be specific for each variable. Commonly, the velocity U is supposed to vary linearly between the wall and the Interpolation Points. The target velocity U_F at the forcing point can therefore be computed using f_{IBC} which is defined as:

$$U_F = f_{IBC}(U_{IntP}) = \frac{d_{FP}}{d_{IntP}} U_{IntP} \quad (6)$$

Where d_{FP} and d_{IntP} are the wall distance at the forcing point and the interpolation point, respectively. This linear hypothesis is valid for detached flow configurations or if the cell size is under $y^+ = 1$. Since the mesh is not especially adapted to the immersed surface, the linear velocity interpolation can be inadequate for high Reynolds number flows. Even with localized refinement techniques, the mesh requirement can be too restrictive [6]. As a consequence IBC are often coupled with wall models to compute high Reynolds numbers flow configuration at an affordable cost. The wall law used in this present work is further described in section 4.

The discrete forcing approach usually requires two layers of forcing cells for classical second-order finite-volume schemes [20]. Here, the second layer is replaced by a face-forcing approach such as the one used in [3, 5, 22] in the specific context of Cartesian finite-volume solvers. For curvilinear grids, the computation of the viscous fluxes requires the variables at each adjacent cell to the face as presented in figure 2. Thus, the first layer of near-wall cells is used to ensure a correct computation of the gradient in the first fluid cells without having to adapt the numerical schemes applied in the fluid domain.

The face forcing approach is designed to modify the MUSCL reconstruction before the computation of the convective fluxes. In the vicinity of the wall, the reconstructed quantities at the cell faces are replaced by the information given by the immersed boundary function f_{IBC} . As presented in figure 3, the reconstructed values

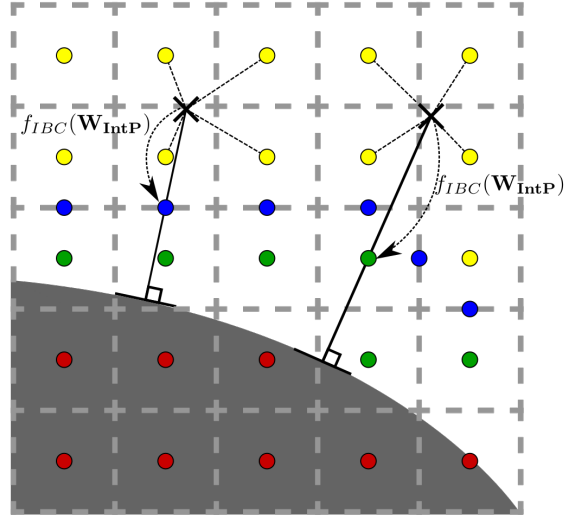


Figure 1: Representation of the forcing procedure for IBC. ● : Fluid cell / ● : Forcing cell / ● : Forcing face / ● : Solid cell / × : Interpolation Point.

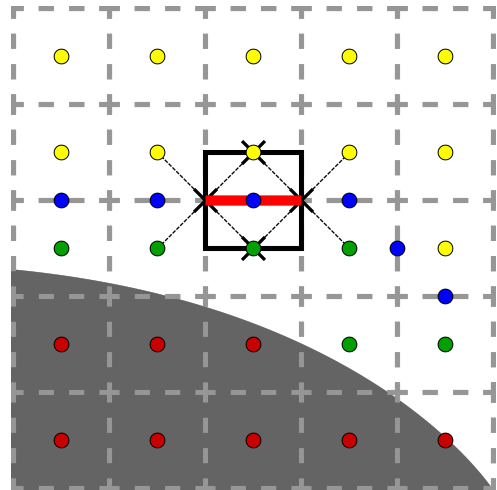


Figure 2: Scheme of the viscous flux computation in the vicinity of the wall. The black square represents the surface used to compute the gradients with a Green-Gauss approach and × the associated quadrature points. The cell nomenclature is the same as in fig. 1.

are changed on the solid side of the cell face. This procedure considerably increases the robustness of the IBC.

Since the second row of fluid cells is removed, the interpolation points can be positioned closer to the interface. Compared with a two-layer IB approach, the wall distance is approximately reduced by 40 %. The wall distance of the interpolation points determines the validity of the boundary condition assumptions. Hence this approach improves this aspect without using a mesh refinement method.

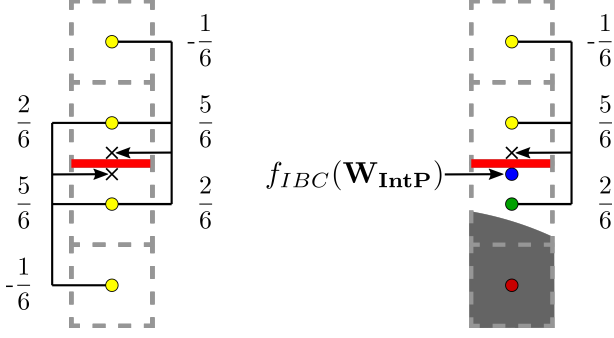


Figure 3: Scheme of the modified state reconstruction for the computation of the inviscid fluxes. (The coefficients correspond to a third-order MUSCL reconstruction.)

Some considerations are required for the interpolation procedure used to reconstruct the variables at the Interpolation Points. A Weighted Least Square (WLSQ) approach is used as described in [18]. For Cartesian meshes the inversion of the systems which is required to compute the WLSQ coefficients is simple and well-conditioned. Yet, for curvilinear grids the inversion of the systems has shown to cause robustness issues. Early works show that the inversion system is far more stable using Singular Value Decomposition (SVD). The matrix A of size $N \times N$, representing the WLSQ system, is first decomposed through SVD as follows :

$$A = U \cdot S \cdot V^T \quad (7)$$

Where U and V are orthogonal matrices of size $N \times N$ and S is a diagonal matrix composed of the singular values. Since the inverse of an orthogonal matrix is its transpose matrix, the inversion of the matrix A is directly given by:

$$A^{-1} = V \cdot S^{-1} \cdot U^T \quad (8)$$

It is worth noticing that this procedure is exclusively made once during the preprocessing operations. The resulting coefficients are stored and used to compute the conservative quantities at the interpolation points. The fluid cells used for the reconstruction procedure are the eight cells surrounding the Interpolation Points. Due to the curvilinearity of the mesh, the identification of these fluid cells can be time-consuming. To speed up this process, it is only carried out in the first 10 layers of cells surrounding the immersed boundaries and a kd-tree architecture [24] is used to get the closest cells of the Interpolation Points.

4. THIN BOUNDARY LAYER EQUATIONS BASED WALL MODEL

In this study, an equilibrium wall model based on TBLE is employed as a boundary formulation for the immersed boundaries. TBLE based wall models have encountered a growing interest and success in the past decades [2, 3, 4, 12]. In contrast with analytical wall models, where the tangential velocity is directly linked to the wall distance, TBLE wall models require to solve simplified RANS equations in the wall-normal direction. Although their computational cost is more expensive [7], the hypotheses are less restraining than with analytical laws. As an example, analytical wall models do not take into account the compressibility effects happening in the turbulent boundary layer. This effect can be partially taken into account with van Driest's transformed and temperature laws as the one proposed by Crocco-Busemann [27]. Nonetheless, these effects are taken into account with TBLE based wall models (see eq (10)).

The present compressible TBLE wall model is based on a set of three diffusion equations :

$$\frac{\partial}{\partial n} \left[(\mu + \mu_t) \frac{\partial u}{\partial n} \right] = 0 \quad (9)$$

$$\frac{\partial}{\partial n} \left[u(\mu + \mu_t) \frac{\partial u}{\partial n} + (\kappa + \kappa_t) \frac{\partial T}{\partial n} \right] = 0 \quad (10)$$

$$c_{b1} \tilde{S} \rho \tilde{v} - \rho c_{w1} f_w \left(\frac{\tilde{v}}{d} \right)^2 + \frac{1}{\sigma} \left(\frac{\partial}{\partial n} \left((\mu + \rho \tilde{v}) \frac{\partial \tilde{v}}{\partial n} \right) + c_{b2} \frac{\partial \tilde{v}}{\partial n} \frac{\partial \rho \tilde{v}}{\partial n} \right) = 0 \quad (11)$$

These equations describe the evolution of the tangential velocity u , the temperature T and \tilde{v} in the wall-normal direction n , respectively. The use of simplified RANS models in addition to TBLE wall models was introduced by Bond and Blottner [2] and has shown to greatly improve the results in comparison with the classical mixing length model. It is worth noticing that the compressible Spalart-Allmaras formulation used in the TBLE formulation (eq (11)) is the same as the one used in the flow solver. During the simulation, the equations (9)-(11) are solved on a one-dimensional mesh (see Fig. 4). Given the wall condition and the flow information at the Interpolation Points the equations (9)-(11) are solved dynamically in order to provide the forcing information leading to the immersed boundary condition.

As stated before, a major drawback of the TBLE approach lies in the resolution cost of each ordinary differential equation (ODE). Initially, Bond and Blottner [2] proposed to solve the TBLE in a decoupled manner with a relaxation factor equal to 0.25. Each system is tridiagonal and can be inverted using Thomas's algorithm [23],

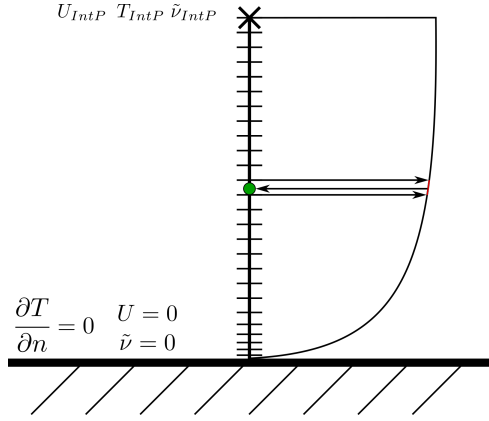


Figure 4: TBLE wall model one-dimensional mesh (● : IB-Forcing Point / × Interpolation Point)

Table 1: List of acronyms used for the different resolution approaches tested and shown in figures 5 and 6

| Abbreviation | Resolution approach |
|--------------|--|
| FC | Fully coupled system |
| FC-A | Fully coupled system with an adaptive Fourier number |
| FD | Fully decoupled system |
| SC | Separated-Coupling |
| SC-A | Separated-Coupling with an adaptive Fourier number |

avoiding to store a full matrix for each TBLE wall model equations. Around four iterations are required to provide a good convergence of the systems for each iteration [4]. Nonetheless, at the initialization of the computation, the convergence of the system requires many iterations. Another possibility relies on the resolution of the fully coupled system. This approach improves the convergence rate of the system greatly but is by far more costly.

The two approaches were tested to assess their convergence properties. The conservative variables from a RANS body-fitted simulation of a flat plate at Mach 2.0 were used as an external boundary condition for the TBLE systems. Figures 5 and 6 present the convergence of the velocity friction and the wall temperature, respectively. As expected, the convergence rate of the fully coupled approach is far better than with the decoupled approach. Nonetheless, the system is by far more costly to solve (see fig. 7).

The main bottleneck, relies on the convergence of equation (10) as it can be seen on the evolution of the wall temperature (see fig. 6). Hence, a new coupling strategy has been adopted in order to improve the convergence rate. The main idea is to uncouple equation (10) while keeping equations (9) and (11) coupled.

Therefore u and \tilde{v} are considered constant during the resolution of equation (10). It should also be noted that μ , μ_t , κ and κ_t depend on the temperature. However, their

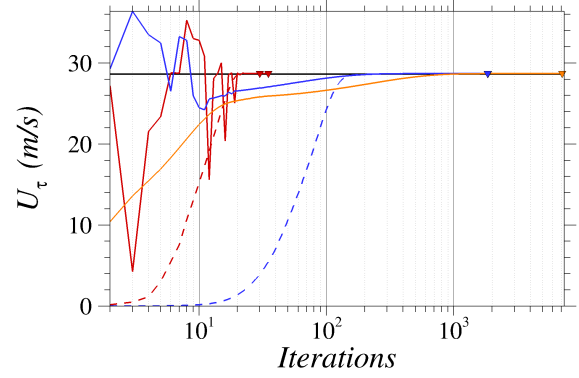


Figure 5: Convergence of the velocity friction and the wall temperature of the TBLE system for different resolution techniques at a Mach number of 2. The symbols show the last iteration of their corresponding method. ---: FC-A / —: FC / ---: SC-A / —: SC / —: FD.

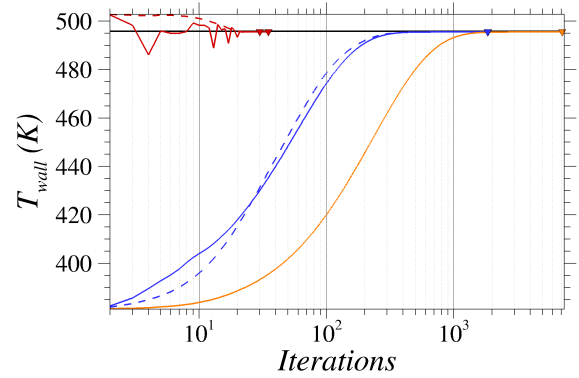


Figure 6: Convergence of the wall temperature of the TBLE system for different resolution techniques at a Mach number of 2. The symbols show the last iteration of their corresponding method. ---: FC-A / —: FC / ---: SC-A / —: SC / —: FD.

variations can be neglected during the inner iterations of the system resolution. As a consequence, the equation (10) can be rewritten:

$$\frac{\partial}{\partial n} \left[C_u + C_\kappa \frac{\partial T}{\partial n} \right] = 0 \quad (12)$$

Where C_κ and C_u are two constants that only depend on the wall distance. These simplifications lead to a linear formulation of equation (10). Therefore, it can be solved without inner iterations with a simple tridiagonal matrix inversion with Thomas's algorithm. This Separated-Coupling (SC) resolution has shown to improve considerably the convergence rate of the TBLE system (fig. 5

and 6) while reducing its computational cost (see fig. 7).

In addition to the present solving strategies, a local and adaptive time step methodology has been used to improve stability during the resolution. Since the TBLE systems only represent the diffusive part of the RANS equations, the Fourier number is used as a stability condition.

$$Fo = \frac{(\mu + \rho \tilde{\nu}) \Delta t}{\rho \Delta x^2} \quad (13)$$

The Fourier number is set to 5 during the first inner iteration. Afterwards, it becomes a function of the residual:

$$Fo^n = \max\left(Fo, Fo\left(\frac{R^0}{R^n}\right)\right) \quad (14)$$

Where R^0 and R^n are respectively the residuals at the first and the current iteration n . This adaptive Fourier approach allows keeping control on the convergence of the system without reducing the convergence properties of the resolution approach (fig. 5 and 6).

The resolution of the TBLE required the generation of one-dimensional meshes to solve equations (9)-(11). In the present simulations, the distance of the first off-wall point and the number of cells are given by the user. Then, an iterative process is used to compute a constant geometric progression between the wall and the IBC Interpolation Point. The mesh generation is not fully automated and requires prior knowledge of the y^+ values. However, such an approach allows reducing the number of points used in the systems while assuring the y^+ criterion for all TBLE systems.

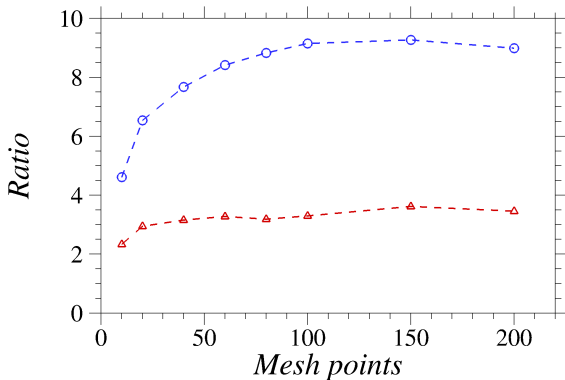


Figure 7: Ratio of the computational cost for one iteration of the TBLE system in function of the cost of the **FD** approach in function of the number of points used for the one-dimensional TBLE mesh. - - - - : FC / - - - - : SC.

5. PRESENTATION OF THE TEST CASE

The "FG5" case is a generic body-tail missile configuration of diameter D and with a length of $16D$. The nose follows a parabolic profile and the fins have a thickness ratio of 6% and a length of $4/3D$ as described in [13, 19, 21]. The sting used in ONERA's experiments has been reproduced in the numerical simulation as presented in figure 8. The freestream Mach number is $M_\infty = 0.8$, and the Reynolds number based on D is $Re_D = 1.3 \times 10^6$ to match ONERA's experiments. The configuration is inclined by an angle of attack of 10° and with a roll angle of 22.5° . These angles introduce a dissymmetrical flow around the fins, making it a particularly complex test case.

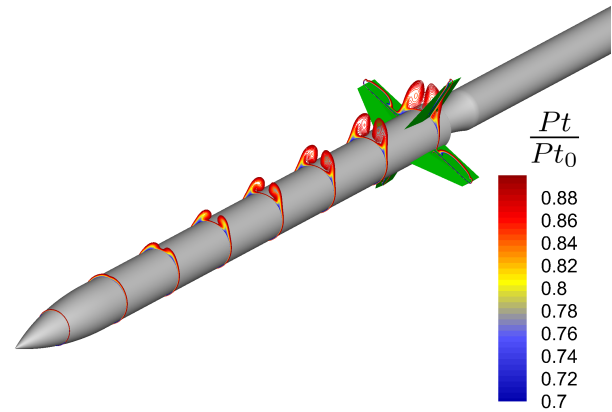


Figure 8: Contour lines of the non-dimensional total pressure for different planes along the FG5 missile configuration of a zonal immersed boundary RANS simulation (grey part: Body-fitted boundary, green part: Immersed Boundary)

Two numerical simulations were conducted on this configuration. The first-one is a full body-fitted simulation with a structured multi-block grid strategy. For each fin, the grid is based on an O-H topology represented in figure 9. This particular topology is designed to avoid a mesh degeneration that could cause significant stability problems. Moreover, this type of topology allows a better resolution of turbulent structures for unsteady simulations. Since the next step of the present work consists of the ZDES [9] simulation of the configuration, this grid topology has been retained. Nonetheless, this grid topology introduces locally twisted cells in the mesh which leads to numerical errors.

The second simulation uses the ZIBC strategy to improve the mesh quality around the fins. As presented in figure 8, these sharp geometric details are introduced with the immersed boundary approach presented in section 3. An O-grid topology has been used to refine the

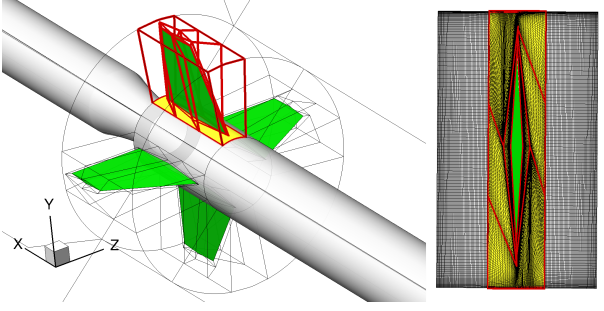


Figure 9: Mesh topology of the full body-fitted grid around the fins

mesh around the fins as presented in figure 10. This strategy significantly reduces the time devoted to the meshing process for this structured grid while improving the mesh quality considerably. Nonetheless, the mesh refinement obtained around the fins is not sufficient to meet the $y^+ = 1$ requirement to simulate the turbulent boundary layer development accurately. As a consequence, the wall model developed in section 4 is used to improve the IBC reconstruction. It is worth noticing that the wall model is only used on the fins. The body and the sting have been meshed with a body-fitted approach with $y^+ < 1$.

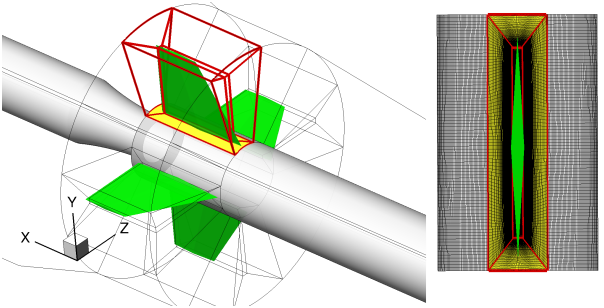


Figure 10: Topology of the grid used around the fins for the simulation using ZIBC

6. RESULTS AND DISCUSSION

The first goal of these simulations is to quantify the impact of the ZIBC strategy on the global load and momentum applied on the configurations. The second objective is to assess the impact of the IBC on the wall pressure field for the entire configuration. Since the flow is transonic, any modification of the flow configuration can change the overall results.

The surface pressure coefficient C_p along the FG5 configuration is plotted with the experimental data for the windward and the leeward side of the configuration, in figures 12 and 11, respectively. In both cases, a good

agreement is obtained with the experiments data for the full body-fitted and the ZIBC simulations.

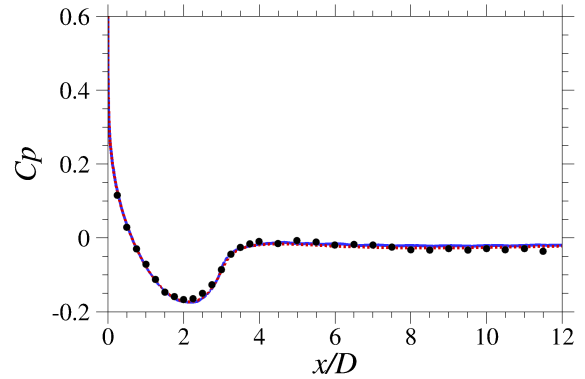


Figure 11: Pressure coefficient along the FG5 configuration at the leeward side. Body-fitted : — / ZIBC : - - - / Experiment : ●.

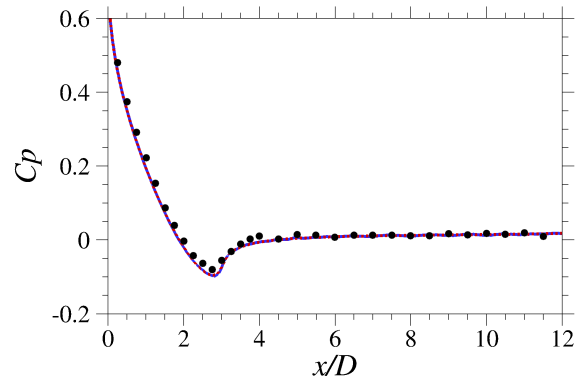


Figure 12: Pressure coefficient along the FG5 configuration at the windward side. — : Body-fitted / - - - : ZIBC / ● : Experiment.

The pressure coefficient in the azimuthal direction at $x/D = 9$ is presented in figure 13. $\Phi = 0^\circ$ coincides with the leeward side and consequently $\Phi = 180^\circ$ with the windward side. At $\Phi \simeq 25^\circ$ a small discrepancy is obtained between the experiment and the simulations. As depicted in figure 8, a separation is obtained all along the configuration. The vortices induced by this phenomenon are the main cause of the pressure drop at $\Phi \simeq 25^\circ$. Even if the point of separation is well predicted, a secondary separation occurred in the experiment which is not retrieved with the present RANS model.

No experimental data were available around the fins. Nonetheless, the main discrepancies between the experiments and the simulations come from the RANS model. As a consequence the ZIBC simulation is supposed to

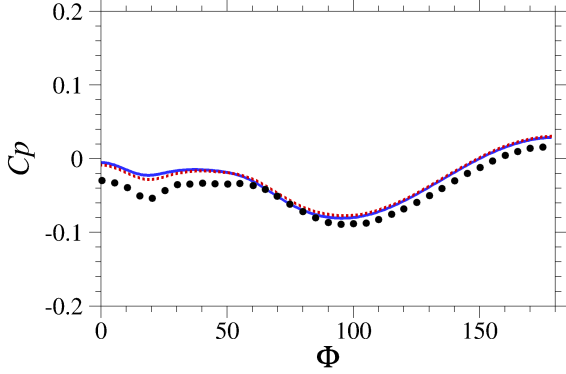


Figure 13: Pressure coefficients at the wall at $x/D = 9$ on the FG5 configuration. Pressure coefficients along the FG5 configuration at the leeward side. — : Body-fitted / - - - : ZIBC / ● : Experiment.

give at best the same results. Therefore a comparison between the two simulations gives information on the accuracy of the present IBC formulation. A visualization of the normalized total pressure P_t has been plotted at $x/D = 15.75$ in figures 14 and 15 for the ZIBC and the body-fitted strategies, respectively. This location is close to the end of the configuration. Consequently, the slice at $x/D = 15.75$ allows to assess the interaction of the wings and the incident flow. Here again, the agreement between the body-fitted and the immersed boundary is satisfying. The main flow features can be observed for both simulations. Moreover, wingtip vortices can be observed for the leeward and the windward fins. Since the mesh quality of the ZIBC strategy is higher than with the full body-fitted simulation, these vortices are less diffused with the ZIBC mesh.

The computation of aerodynamic forces has been assessed on the body-tail configuration (i.e. without the sting) for both simulations. The computation of the load applied on immersed boundaries is far from being trivial [1]. In practice the results depicted in figure 16, are computed using the approach presented in [14] and detailed in [15]. An overall good agreement is found between the body-fitted approach and the ZIBC strategy. The load and momentum components present a relative difference lower than 4%. The greatest gap is on the axial force coefficient (CA), which is mainly influenced by the friction coefficient. Finally, the main discrepancies with the experiments come with the yawing moment coefficient. The RANS hypothesis fails to be representative of this phenomenon. Nonetheless, the relevant quantities such as the aerodynamic coefficients are well reproduced with both the present ZIBC strategy and a body-fitted strategy.

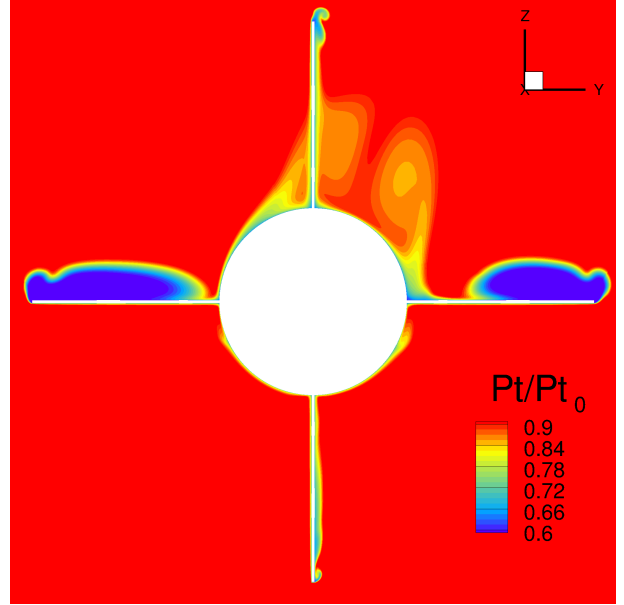


Figure 14: Slice of the total pressure normalized with the freestream value at $x/D=15.75$ for the ZIBC simulation

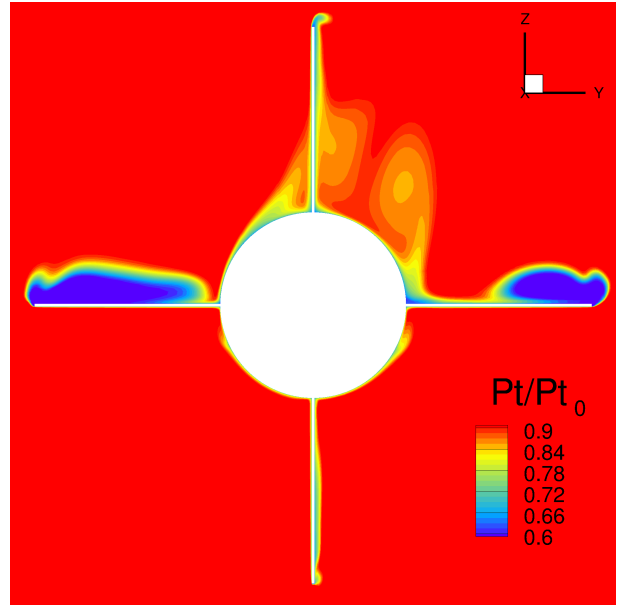


Figure 15: Slice of the total pressure normalized with the freestream value at $x/D=15.75$ for the full body-fitted simulation

7. CONCLUSION

A FG5 missile configuration with an angle of attack of 10° and a roll angle of 22.5° has been simulated. The transonic RANS simulation has been performed with a zonal application of IBC to simplify the mesh generation

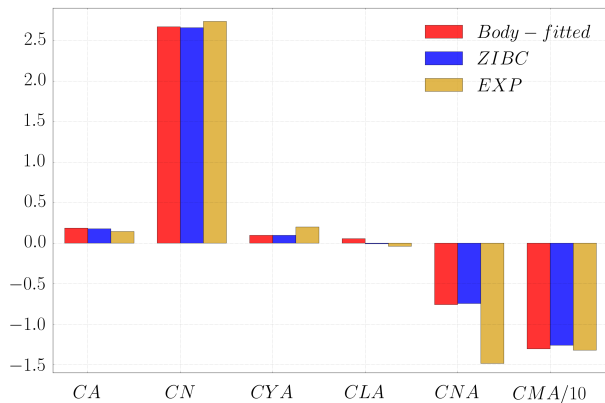


Figure 16: Plot of the aerodynamic load and momentum coefficients for the FG5 configuration

process on this configuration. In particular, a new compact IBC formulation coupled with a TBLE wall model incorporating the S-A model has been used in the ZIBC numerical strategy to improve the simulation of compressible turbulent boundary layers. This approach has shown to adequately generate the effect of the fins in the simulation. Moreover, the strategy developed in [14] has allowed to correctly compute the aerodynamic load and momentum on the entire configuration. In future work, this configuration with the same mesh strategies will be simulated using a Zonal Detached Eddy Simulation approach [9, 10] to investigate the new IBC approach for unsteady simulations.

REFERENCES

- [1] A. Bharadwaj and S. Ghosh. Data reconstruction at surface in immersed-boundary methods. *Computers & Fluids*, 196:104236, January 2020.
- [2] R. B. Bond and F. G. Blottner. Derivation, implementation, and initial testing of a compressible wall-layer model. *International Journal for Numerical Methods in fluids*, 66:1183–1206, 2011.
- [3] C. Brehm and N. Ashton. Towards a viscous wall model for immersed boundary methods. In *2018 AIAA Aerospace Sciences Meeting*. American Institute of Aeronautics and Astronautics, jan 2018.
- [4] F. Capizzano. Coupling a wall diffusion model with an immersed boundary technique. *AIAA Journal*, 54(2):728–734, 2016.
- [5] F. Capizzano. Automatic generation of locally refined cartesian meshes: Data management and algorithms. *International Journal for Numerical Methods in Engineering*, 113(5):789–813, sep 2017.
- [6] F. Capizzano, L. Alterio, S. Russo, and C. de Nicola. A hybrid RANS-LES cartesian method based on a skew-symmetric convective operator. *Journal of Computational Physics*, 390:359–379, August 2019.
- [7] M. Catchirayer, J.-F. Boussuge, P. Sagaut, M. Montagnac, D. Papadogiannis, and X. Garnaud. Extended integral wall-model for large-eddy simulations of compressible wall-bounded turbulent flows. *Physics of Fluids*, 30(6):065106, jun 2018.
- [8] S. R. Chakravarthy. High resolution upwind formulation of the navier-stokes equations. In *Cours VKI, Lecture Series*, 1988.
- [9] S. Deck. Recent improvements in the Zonal Detached Eddy Simulation (ZDES) formulation. *Theoretical and Computational Fluid Dynamics*, 26(6):523–550, 2012.
- [10] S. Deck and N. Renard. Towards an enhanced protection of attached boundary layers in hybrid rans/les methods. *Journal of Computational Physics*, 400, 2020.
- [11] E.A. Fadlun, R. Verzicco, P. Orlandi, and J. Mohd-Yusof. Combined immersed-boundary finite-difference methods for three-dimensional complex flow simulations. *Journal of Computational Physics*, 161(1):35–60, 2000.
- [12] Y. Fukushima and S. Kawai. Wall-modeled large-eddy simulation of transonic airfoil buffet at high reynolds number. *AIAA Journal*, pages 1–18, apr 2018.
- [13] M. Lyonnet. tude du roulis induit de configurations gnriques de missiles dans la soufflerie S3MA. Technical report, ONERA, 1992.
- [14] L. Manueco, P.-É. Weiss, and S. Deck. Towards the prediction of fluctuating wall quantities using immersed boundary conditions. In *AIAA Aviation 2019 Forum*. American Institute of Aeronautics and Astronautics, June 2019.
- [15] L. Manueco, P.-É. Weiss, and S. Deck. On the estimation of unsteady aerodynamic forces and wall spectral content with immersed boundary conditions. *Computers & Fluids*, 201:104471, 2020.
- [16] L. Mochel, P.-É. Weiss, and S. Deck. Zonal immersed boundary conditions: Application to a high-Reynolds-number afterbody flow. *AIAA Journal*, 52(12):27822794, 2014.
- [17] J. Mohd-Yusof. Development of immersed boundary methods for complex geometries. *Center for Turbulence Research, Annual Research Briefs*, pages 325–336, 1998.

- [18] A. Nealen. An as-short-as-possible introduction to the least squares, weighted least squares and moving least squares methods for scattered data approximation and interpolation. *URL: <http://www.nealen.com/projects>*, 130(150):25, 2004.
- [19] J. E. Peter, S. Goertz, and R. E. Graves. Three-parameter uncertainty quantification for generic missile FG5. In *55th AIAA Aerospace Sciences Meeting*, 2017.
- [20] A. Piquet, O. Roussel, and A. Hadjadj. A comparative study of brinkman penalization and direct-forcing immersed boundary methods for compressible viscous flows. *Computers & Fluids*, 136:272–284, 2016.
- [21] B. Prananta, S. Deck, P. d’Espiney, A. Jirasek, A. Kovar, M. Leplat, C. Nottin, K. Petterson, and I. Wrisdale. Numerical simulations of turbulent subsonic and transonic flows about missile configurations Final report of the GARTEUR (AD) AG42 Missile Aerodynamics. *GARTEUR LIMITED*, TP-166, 2008.
- [22] Y. Tamaki and T. Imamura. Turbulent flow simulations of the common research model using immersed boundary method. *AIAA Journal*, pages 1–12, apr 2018.
- [23] L.H. Thomas. Watson sci. comput. lab report, 1949.
- [24] I. Wald and V. Havran. On building fast kd-trees for ray tracing, and on doing that in $O(n \log n)$. In *2006 IEEE Symposium on Interactive Ray Tracing*. IEEE, sep 2006.
- [25] P.-É. Weiss. ZDES of an Ariane 6 PPH configuration with incidence angle using Zonal Immersed Boundary Conditions. In *European Conference for Aeronautics and Space Sciences. Madrid, Spain*. Proceedings of the 8th European Conference for Aeronautics and Space Sciences. Madrid, Spain, 1-4 july 2019, 2019.
- [26] P.-É. Weiss and S. Deck. On the coupling of a zonal body-fitted/immersed boundary method with ZDES: Application to the interactions on a realistic space launcher afterbody flow. *Computers & Fluids*, 176:338–352, nov 2018.
- [27] F. M. White and I. Corfield. *Viscous fluid flow*, volume 3. McGraw-Hill New York, 2006.